medRxiv preprint doi: https://doi.org/10.1101/2020.11.17.20233403; this version posted June 7, 2021. The copyright holder for this preprint (which was not certified by peer review) is the author/funder, who has granted medRxiv a license to display the preprint in perpetuity. It is made available under a CC-BY 4.0 International license .

The stochastic dynamics of early epidemics: probability of establishment, initial growth rate, and infection cluster size at first detection

Peter Czuppon[1,2,3], Emmanuel Schertzer[4], François Blanquart[2,5,*], Florence Débarre[1,*]

[1] Institute of Ecology and Environmental Sciences of Paris (iEES-Paris, UMR 7618), Sorbonne Université, CNRS, UPEC, IRD, INRAE, 75252 Paris, France

[2] Center for Interdisciplinary Research in Biology, CNRS, Collège de France, PSL Research University, 75005 Paris, France

[3] Institute for Evolution and Biodiversity, University of Münster, 48149 Münster, Germany

[4] Faculty of Mathematics, University of Vienna, 1090 Wien, Austria

[5] Université de Paris, INSERM, IAME, 75018 Paris, France

[*] equal contributions

NOTE: This preprint reports new research that has not been certified by peer review and should not be used to guide clinical practice.

medRxiv preprint doi: https://doi.org/10.1101/2020.11.17.20233403; this version posted June 7, 2021. The copyright holder for this preprint (which was not certified by peer review) is the author/funder, who has granted medRxiv a license to display the preprint in perpetuity. It is made available under a CC-BY 4.0 International license .

Abstract. Emerging epidemics and local infection clusters are initially prone to stochastic effects that can substantially impact the epidemic trajectory, even in the long term. While numerous studies are devoted to the deterministic regime of an established epidemic, mathematical descriptions of the initial phase of epidemic growth are comparatively rarer. Here, we review existing mathematical results, and derive new results, to elucidate the early dynamics of an infection cluster started by a single infected individual. We cover the probability of establishment of an epidemic as a function of the distribution of secondary cases, the expectation of epidemic size as a function of time, and the convergence to a deterministic exponential regime. Stochasticity systematically accelerates the initial growth of an epidemic, because epidemics that do not get extinct have faster initial growth on average. This also affects the long-term epidemic growth by increasing the cumulative size by a constant factor, the inverse of the establishment probability, when compared to the deterministic prediction. These results are critical to improve early cluster detection and control. We compute the probability distribution of the first detection time of an infected individual in an infection cluster depending on the testing effort (assumed to be constant in time), and estimate that the SARS-CoV-2 variant of concern B.1.1.7 detected in September 2020 first appeared in the United Kingdom early August 2020. We estimate a minimal testing frequency to detect clusters before they exceed a certain threshold size, and we compute the detection rate of infected individuals during a single mass testing effort. For example, in a COVID-19-parameterized model with an effective reproduction number $R = 1.1$, a fraction 1.3% of a population needs to be randomly tested each day for cluster size to not exceed 30 infected individuals. These results improve our theoretical understanding of early epidemics and will be useful for the study and control of local infectious disease clusters.

Keywords: early epidemic dynamics, establishment probability, renewal equation, mass testing, timing of detection, testing frequency

medRxiv preprint doi: https://doi.org/10.1101/2020.11.17.20233403; this version posted June 7, 2021. The copyright holder for this preprint (which was not certified by peer review) is the author/funder, who has granted medRxiv a license to display the preprint in perpetuity. It is made available under a CC-BY 4.0 International license .

1 Introduction

The emergence and spread of infectious diseases pose an increasing threat in an ever more interconnected world. A quantitative understanding of epidemic dynamics is necessary to improve control measures. Deterministic models are a suitable tool to describe the epidemiological dynamics once a large number of individuals has been infected. During the early phase of an epidemic or a local infection cluster however, stochastic effects cannot be neglected. These stochastic effects are due to the initially low number of infected individuals, and to the inherent stochasticity of the transmission process. Understanding and quantifying these stochastic effects will help, for example, assess the risk of new infection clusters emerging or estimate the size of a cluster associated to a new variant when such a variant is detected.

The infectiousness of an infectious disease may vary over the course of infection. We consider a generic stochastic model with an arbitrary age of infection dependent infectiousness. This stochastic model is called a general branching process or Crump-Mode-Jagers process (Crump and Mode, 1968, 1969; Jagers, 1969). When the number of infected individuals gets large, this stochastic model can be approximated by a deterministic partial differential equation describing the infection age distribution of the host population. This equation is known as the McKendrick-von Foerster partial differential equation (McKendrick, 1925; Diekmann and Heesterbeek, 2000; Foutel-Rodier et al., 2020).

Transmission timings are particularly influential during the early stages of the growth of an infection cluster, which is the focus of our work, so it is important to use biologically realistic distributions of transmission times rather than assuming mathematically convenient but biologically unrealistic exponential distributions (e.g. Linton et al., 2020). A constant infectiousness over the duration of an individual's infection leads to the predominantly used framework of ordinary differential equations, while non-constant infectiousness can be captured by a partial differential equation. In addition to the added biological realism, a time-varying infectiousness of infected individuals can also properly capture the dynamical consequences of abrupt changes in the transmission rate (e.g. Foutel-Rodier et al., 2020; Forien et al., 2021). This is not possible with an ordinary differential equation framework (e.g. Gatto et al., 2020).

In this manuscript, we provide key results about the establishment probability of an infection cluster and the epidemic dynamics as described by the McKendrick-von Foerster equation. We confirm that the establishment probability of a new local cluster strongly depends not only on the average number of secondary infections, also referred to as the basic/effective reproduction number denoted by R, but also on the full distribution of secondary infections, which accounts for the probability of superspreading events. This stochasticity in transmission does not merely add noise to the dynamics, but also causes a systematic deviation from the deterministic description, which underestimates the initial growth of the epidemic size (Mercer et al., 2011; Rebuli et al., 2018). This is in contradiction to a common misconception that stochasticity generally slows down the initial epidemic growth rate. We quantify the deviation between the deterministic and observed stochastic growth rate by conditioning the individual-based process on survival. After initial stochastic effects, the process converges to exponential growth with an asymptotic growth rate, denoted r, derived from the reproduction number R and the transmission rate. The distribution of age of infection in the stationary regime is exponential with parameter r, the asymptotic growth rate.

The reviewed and newly derived results can provide answers to public health related questions. How many importations will eventually result in a local infection cluster? How large is a local cluster once a first case is detected? When did a new variant – like B.1.1.7 first detected in the United Kingdom (UK) – arise? How large is the detection rate of infectious individuals by a single mass testing effort? How many daily tests need to be conducted to detect local clusters before they exceed a certain size? We will show how our theoretical results provide quantitative answers to these questions.

medRxiv preprint doi: https://doi.org/10.1101/2020.11.17.20233403; this version posted June 7, 2021. The copyright holder for this preprint (which was not certified by peer review) is the author/funder, who has granted medRxiv a license to display the preprint in perpetuity. It is made available under a CC-BY 4.0 International license .

2 Probability of establishment

Introductions of infected individuals into a susceptible population do not always result in a local infection cluster because of random extinction. Here, we quantify the chance that the introduction of a single infected individual results in the establishment of a local cluster. The establishment probability of a local cluster depends on the probability distribution of the number of secondary infections, which also determines the chance of superspreading events. Similarly, the initial spread of new variants can be modeled just as emerging clusters. In the following, we briefly outline how to compute the probability of establishment and study how it is affected by different types of transmission distributions.

In our epidemiological model, we assume that the number of susceptible individuals is not limiting the spread of the disease, i.e., that the fraction of susceptible individuals in the population remains close to one. Every infected individual transmits the disease to R other individuals on average, where R is the effective reproduction number. The actual number of secondary infections can vary strongly between infected individuals. For example, estimates for COVID-19 indicate that about 20% of infected individuals are responsible for about 80% of secondary infections (Endo et al., 2020). These superspreaders (or superspreading events) cannot be captured by a Poisson-distributed number of secondary infections (Lloyd-Smith et al., 2005). A more dispersed distribution, i.e. with a larger variance, is the negative binomial distribution, where most of infected individuals do not transmit the disease at all. Its variance is typically quantified by the dispersion parameter $\kappa > 0$. The smaller the value of κ, the more variance has the negative binomial distribution.

The establishment probability of a local cluster can be computed by following the transmission chain from one generation of infected individuals to the next. Specifically, if Y is the random number of secondary infections due to one infected individual, the probability of extinction, i.e., 1 minus the probability of survival, is computed by summing over the possible numbers of secondary infections times the probability that all corresponding chains of transmission do not survive:

$$p_{\text{ext}} = \underbrace{\mathbf{P}(Y=0)}_{\substack{\text{no secondary}\\ \text{infection}}} + \underbrace{p_{\text{ext}}\mathbf{P}(Y=1)}_{\substack{\text{one secondary}\\ \text{infection}}} + \underbrace{p_{\text{ext}}^2\mathbf{P}(Y=2)}_{\substack{\text{two secondary}\\ \text{infections}}} + p_{\text{ext}}^3\mathbf{P}(Y=3) + \cdots = \mathbf{E}[p_{\text{ext}}^Y]\,. \tag{1}$$

The expectation on the right, $\mathbf{E}[z^Y]$, is called the probability generating function and can be computed for several distributions explicitly. Eq. (1) then shows that the probability of extinction p_{ext} of a cluster started with a single infected individual, is given by the smallest positive fixed point of the probability generating function, i.e., $\mathbf{E}[z^Y] = z$ (Haccou et al., 2005). If the epidemic is started with k infected individuals, the extinction probability is simply given by p_{ext}^k, which yields a survival probability of $p_{\text{surv}} = 1 - p_{\text{ext}}^k$. Here, and also in the first equality of Eq. (1), we have used the assumption that the transmission chains of the k initially infected individuals are independent of each other.

Plugging in different distributions for the number of secondary infections, we can numerically compute the probability of extinction. In the particular case of a geometric distribution, which is a negative binomial distribution with dispersion parameter $\kappa = 1$ (compare to Eq. (3) below), the fixed point equation can be solved analytically by

$$\mathbf{E}[z^Y] = \frac{p}{1-(1-p)z} \quad \Rightarrow \quad p_{\text{ext}} = \frac{p}{1-p} = \frac{1}{R}, \tag{2}$$

where p is the success probability of the geometric distribution and R is the average number of secondary infections (or effective reproduction number). The last equality in Eq. (2) is obtained by noting that R is equal to the the mean of the distribution, and that the mean of a geometric distribution is $(1-p)/p$.

medRxiv preprint doi: https://doi.org/10.1101/2020.11.17.20233403; this version posted June 7, 2021. The copyright holder for this preprint (which was not certified by peer review) is the author/funder, who has granted medRxiv a license to display the preprint in perpetuity. It is made available under a CC-BY 4.0 International license .

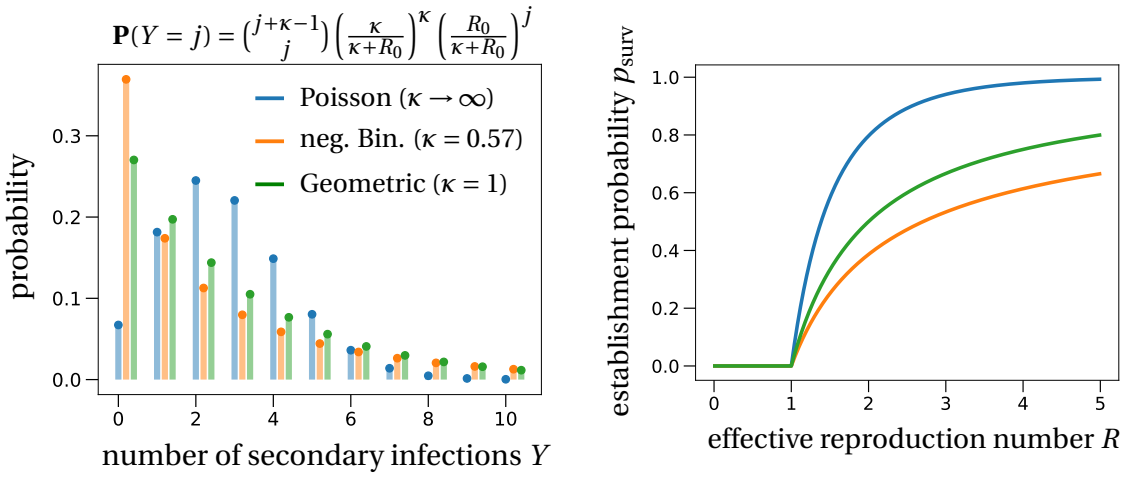

(a) Distribution of secondary infections

(b) Establishment probability

Figure 1: **Probability distribution and establishment probability of an epidemic for different distributions of the number of secondary infections.** (a) The probability for an infected individual to transmit the disease to Y susceptible individuals depends on the distribution of the number of secondary infections. The probability to not transmit the disease ($Y = 0$) is highest for the negative binomial distribution with $\kappa = 0.57$ (orange bars; value estimated for the French COVID-19 data pre-lockdown 2020; Salje et al. (2020)), i.e., the distribution with the highest variance. The probability of establishment is smallest for the offspring distribution with the largest variance, as shown in (b). For $\kappa = 1$, the geometric distribution (green curve), the establishment probability is explicit: $p_{\mathrm{surv}} = 1 - 1/R$. The largest establishment probability is found for a Poisson-distributed number of secondary transmission events (blue curve).

The probability generating functions for the negative binomial and the Poisson distributions are given by

$$\mathbf{E}[z^Y] = \begin{cases} \left(\frac{p}{1-(1-p)z}\right)^{\kappa}, & \text{neg. binomial dist. with mean } R \text{ and dispersion parameter } \kappa \\ & \text{(success probability } p = \frac{\kappa}{\kappa+R}), \\ e^{R(z-1)}, & \text{Poisson distribution with mean } R. \end{cases} \tag{3}$$

Note that the Poisson distribution is obtained from the negative binomial distribution in the limit $\kappa \to \infty$. The fixed point of the probability generating functions of a negative binomial or a Poisson distribution cannot be computed analytically.

In Fig. 1, we plot the distributions and establishment probabilities as a function of R for the three different distributions of number of secondary infections. For R smaller than 1, the epidemic will not establish, so that the establishment probability is 0. For values of the effective reproduction number R greater than 1, the establishment probability becomes positive and the epidemic has a chance to establish. In general, the smaller the offspring variance, i.e., the larger the dispersion parameter κ of the negative binomial distribution, the larger the probability of establishment. In applications, the analytically exact result $1/R$ (Eq.(2)) is often used to approximate the extinction probability of an epidemic. Fig. 1 shows that this is indeed a reasonably good approximation for overdispersed offspring distributions such as the negative binomial distribution with a parameter $\kappa < 1$, at least as long as R does not become too large.

medRxiv preprint doi: https://doi.org/10.1101/2020.11.17.20233403; this version posted June 7, 2021. The copyright holder for this preprint (which was not certified by peer review) is the author/funder, who has granted medRxiv a license to display the preprint in perpetuity. It is made available under a CC-BY 4.0 International license .

3 Expected epidemic size

We now study the epidemic size of a cluster initiated by a single infected individual. Because some of our developments will also need them, we first recall results on *deterministic* epidemiological dynamics, then develop new analytical results on the expected early growth and the expected number of infected individuals once a stationary regime has been reached. We illustrate with simulations the variability across stochastic trajectories (Fig. 2). As observed before (Mercer et al., 2011; Rebuli et al., 2018), the expected growth rate during the early phase of cluster growth is greater than the long-term deterministic expectation, because clusters that do not die out are typically those that initially grow faster. We show how to account for this phenomenon in the mathematical description of the early phase and of the stationary regime.

In our stochastic simulations, we assume that the epidemic starts with a single infected individual at time $t = 0$. Each infected individual i is assigned an infection age a_i measuring the time since the individual was infected. The age of infection determines the infectiousness of an individual through time. We decouple the transmission rate $\tau(t)$ into the mean number of secondary infections R and the transmission probability density over time $\mu(t)$. We then have

$$\tau(t) = R \times \mu(t). \tag{4}$$

This equation holds because $\int_0^\infty \mu(t)dt = 1$ (μ is a probability density), so that indeed the average number of secondary infections is given by R. This decoupling allows us, in a relatively simple way, to study different offspring distributions for R, while leaving the transmission density $\mu(t)$ unchanged.

For illustration, we assume that the distribution of transmission times follows a gamma distribution, but our framework is sufficiently general to account for any distribution. In particular, a constant transmission rate would result in an exponential distribution of the transmission times (i.e., the memory-less distribution), which would reduce this general model into an ordinary differential equation (ODE).

3.1 Previous results on deterministic dynamics: renewal equation, growth rate and age-of-infection distribution

Throughout our analysis, we assume that the fraction of susceptible individuals is sufficiently large compared to the number of individuals infected in the early epidemic that it remains approximately constant. The overall rate at which new infections occur at time t, denoted by $i(t)$, in the deterministic regime is described by the following renewal equation (e.g Wallinga and Lipsitch, 2006):

$$i(t) \;=\; \tau(t) \;+\; \int_0^t \tau(a)i(t-a)da, \tag{5}$$

where $\tau(a)$ is the transmission rate of an individual with infection age a. The first term $\tau(t)$ reflects the new infections by the first infected individual at time t. The integral in Eq. (5) is the continuous version of the sum over the number of new infections caused by individuals with age of infection a ($i(t-a)da$), which happens at rate $\tau(a)$. Intuitively, one can think about $i(t)dt$ being the incidence at time t, i.e., the number of newly infected individuals in the small time interval $[t, t+dt]$.

The cumulative number of infected individuals, i.e., the total epidemic size, which we denote by $I(t)$, is then given by

$$I(t) = 1 + \int_0^t i(s)ds = 1 + \int_0^t I(t-a)\tau(a)da, \tag{6}$$

with $I(0) = 1$ (mathematical details are given in Appendix C). For simplicity, we do not consider recovery of infected individuals. However, individuals will of course stop transmitting when the age of infection is such that the transmission rate $\tau(a)$ becomes very small.

medRxiv preprint doi: https://doi.org/10.1101/2020.11.17.20233403; this version posted June 7, 2021. The copyright holder for this preprint (which was not certified by peer review) is the author/funder, who has granted medRxiv a license to display the preprint in perpetuity. It is made available under a CC-BY 4.0 International license .

The epidemic size $I(t)$ will, for large times t, grow exponentially if $R > 1$. Formally, the asymptotic exponential growth rate r is obtained by solving the classical Euler-Lotka equation (e.g. Wallinga and Lipsitch, 2006; Britton and Tomba, 2019):

$$1 = \int_0^\infty e^{-rt}\tau(t)dt \quad \Leftrightarrow \quad \frac{1}{R} = \int_0^\infty e^{-rt}\mu(t)dt, \tag{7}$$

where r is also called the Malthusian parameter of the supercritical branching process (Athreya and Ney, 1972; Haccou et al., 2005). In the case where $\mu(t)$ is given as the density of a gamma distribution with shape parameter α and scale parameter β, the exponential growth rate r is

$$r = \frac{R^{1/\alpha} - 1}{\beta}. \tag{8}$$

Convergence speed from the initial condition towards the asymptotic growth rate r is determined by the average number of secondary infections R and the transmission probability density μ. Intuitively, the faster a large number of infected individuals is reached (high R and/or small average transmission time), the faster is the convergence towards the stationary growth regime.

Furthermore, it is possible to derive an explicit expression for the number of infected individuals over time, once asymptotic growth is reached. It follows from results of supercritical general branching processes and renewal theory, e.g. Haccou et al. (2005, Section 3.3.1), that the expected cumulative epidemic size is, for asymptotically large times t, given by

$$I(t) = I(0)\frac{e^{rt}}{rR\int_0^\infty e^{-rs}s\mu(s)ds}. \tag{9}$$

The integral in the denominator is the mean generation time of the Malthusian process (Svensson, 2007; Britton and Tomba, 2019). This is the time between the infection of the infecting individual and the time of infection of a randomly chosen secondary infection event. If the transmission density $\mu(s)$ were constant (note that formally then μ is not a probability density anymore), the integral would be $1/(rR)$ and the epidemic size would be the solution of a constant infection process without depletion of susceptibles: $I(t) = I(0)e^{rt}$.

For an uncontrolled COVID-19-epidemic (we set $R = 2.9$ according to Salje et al. (2020), estimated for the French epidemic in Spring 2020), we obtain $r \approx 0.18$ per day, which corresponds to a doubling time of about 4 days (the value is computed by solving $2 = e^{rt_{\text{doubling}}}$ for t_{doubling}). When interventions are in place (e.g., $R = 1.3$), then the Malthusian parameter is $r \approx 0.048$ per day, which corresponds to a doubling time of 14 days.

Under exponential growth, the distribution of the ages of infection in the population is given by an exponential distribution with parameter r, the exponential growth rate (e.g. Haccou et al., 2005, Section 3.4). Intuitively, in an exponentially growing population, the number of individuals who were infected a days ago is e^r times greater than the number of individuals who were infected $a+1$ days ago. The exponential distribution also implies that for a large growth rate r, a large proportion of the cumulative number of infections will be very recent. For example, with $R = 2.9$, the proportion of infections that occurred within the last two days, among the total cumulative number of infections, is around 30%, as long as the average number of secondary infections R remains stable. For a value of $R = 1.3$ on the other hand, this proportion is only at 9%.

We now turn to the stochastic simulations and show how systematic deviations from the deterministic regime can be understood and mathematically described. We first give a stochastic correction for the asymptotic growth rate and then apply a similar idea to the general epidemic size process over time.

medRxiv preprint doi: https://doi.org/10.1101/2020.11.17.20233403; this version posted June 7, 2021. The copyright holder for this preprint (which was not certified by peer review) is the author/funder, who has granted medRxiv a license to display the preprint in perpetuity. It is made available under a CC-BY 4.0 International license .

3.2 Asymptotic growth rate and epidemic size in the stochastic epidemic model

For large enough times after the initially infected individual started the local cluster, the epidemic grows exponentially at the rate predicted by the Euler-Lotka equation (Eq. (7)). However, the expected cumulative epidemic size derived for the deterministic case (Eq. (9)) includes epidemics that eventually die out. Since we are only interested in epidemic clusters that eventually result in a large epidemic outbreak, we rescale the initial epidemic size by dividing by the survival probability $p_{\text{surv}} = 1 - p_{\text{ext}}$:

$$I_{\text{surv}}(t) = \frac{I(t)}{p_{\text{surv}}} = \frac{I(0)}{p_{\text{surv}}} \frac{e^{rt}}{rR\int_0^\infty e^{-rs} s\mu(s)ds} . \tag{10}$$

This rescaling reflects conditioning of the epidemic process on survival (Fig. 2). The survival probability p_{surv} can be found by numerically computing the fixed point of the probability generating function of the offspring distribution, as outlined in Section 2.

Formally, this correction of the asymptotic limit is derived from a convergence result of a general branching process (Appendix B). It is a standard result in branching process theory that conditional on survival, the number of infected individuals at time t rescaled by e^{rt} converges to a limiting random variable with mean $1/p_{\text{surv}}$ (Eq. (B.5) in Appendix B). As a consequence, the term $I(0)/p_{\text{surv}}$ in Eq. (10) is the mean of this limiting random variable conditioned on survival. More generally, we can also compute the variance and higher moments of this limit, yet, we do not obtain its whole distribution. For this reason, we will reduce our analysis to the mean of this process, as given in Eq. (10), and only state the more general results in Appendix B.

3.3 Initial stochastic growth of an epidemic

The initial growth rate of an epidemic that does not get extinct is initially steeper than its final asymptotic growth rate (Mercer et al., 2011; Rebuli et al., 2018) (compare the initial slope of the mean of stochastic simulations with the asymptotic growth for large times; gray dots vs. blue solid line in Fig. 2). This is due to the inherent stochasticity of the transmission process, which strongly affects the dynamics when there are only a small number of infected individuals. Clusters that escape extinctions are typically those that by chance benefited from a larger initial growth than the long-term expectation. This also means that deterministic models tend to underestimate epidemic sizes early on, or, if parameters are inferred from data, overestimate epidemic parameters such as the true basic reproduction number R_0, as for example observed in Kochańczyk et al. (2020).

To account for this initial stochastic phase, one can alter the individual-based dynamics by conditioning the stochastic process on the survival of the epidemic. A similar procedure has been employed in Rebuli et al. (2018). This conditioning results in an adjustment of the transmission rate τ, which we denote by $\widetilde{\tau}$. Formally, this adjustment is only justified for the stochastic process by Doob's h-transform (Doob, 1957; Chetrite and Touchette, 2015) (more details are given in Appendix D). In the large population size limit, we then approximate the adjusted transmission rate by the continuous analog of the adjusted transmission rate of the stochastic process. This approximation, while mathematically not fully justified, is a natural analogy of the conditioning of the asymptotic epidemic size in Eq. (10). The mean epidemic size of the adjusted process is then computed by

$$\widetilde{I}(t) = 1 + \int_0^t \widetilde{i}(s)ds, \tag{11}$$

where $\widetilde{i}(s)ds$ is the incidence in the time interval $[s, s+ds)$ under the adjusted process. The rate of new infections $\widetilde{i}(t)$ in the conditioned process now depends non-linearly on the history of the epidemic and

medRxiv preprint doi: https://doi.org/10.1101/2020.11.17.20233403; this version posted June 7, 2021. The copyright holder for this preprint (which was not certified by peer review) is the author/funder, who has granted medRxiv a license to display the preprint in perpetuity. It is made available under a CC-BY 4.0 International license .

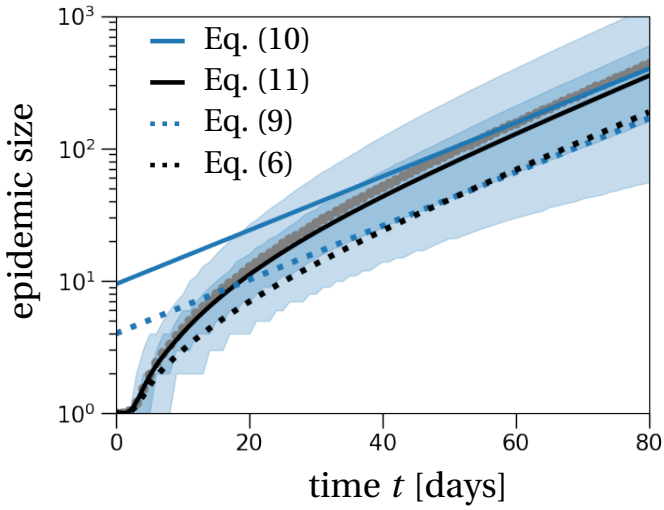

Figure 2: **The cumulative number of infected individuals over time.** The light and dark shaded regions show the 90% and 50% inter-quantile ranges obtained from 10,000 stochastic simulations that resulted in cluster establishment. Gray dots show the average of these simulations over time. The theoretical prediction (black solid line) is calculated from Eq. (11) with the adjusted transmission rate as computed in Appendix D. The black dotted line shows the prediction obtained from Eq. (6) without the conditioning for the epidemic to establish. The solid blue line is the epidemic size predicted by the asymptotic growth rate as stated in Eq. (10). The blue dotted line is the corresponding quantity without the stochastic adjustment (Eq. (9)). The effective reproduction number is set to $R = 1.3$, the number of secondary transmission events is Poisson-distributed, and the transmission density $\mu(t)$ is a Gamma distribution with the parameters given in Table 1.

therefore does not satisfy a renewal equation as in Eq. (5), but a delay differential equation equation:

$$\widetilde{i}(t) = F(\widetilde{i}(s); s \in [0, t]) \,. \tag{12}$$

The function F is explicitly computed in Appendix D (Eq. (D.12)). In short, the conditioning on survival of the epidemic results in an adjustment of the transmission rate τ by a factor that varies over time. This adjustment factor reflects the survival probability of the epidemic at a certain time and therefore depends on the size and the age structure of the epidemic over time. The adjustment factor is largest at time $t = 0$, where it equals $(1 + p_{\text{ext}})$. Over time, the adjustment factor decreases and asymptotically approaches 1 for a large epidemic size, where the probability of extinction becomes negligible. For large times t, we therefore have $\widetilde{\tau} = \tau$.

In Fig. 2, we plotted both the adjusted and non-adjusted versions of the mean epidemic size (Eqs. (6) and (11)). As mentioned above, the non-adjusted formula (black dotted line) underestimates the mean epidemic sizes as obtained from 10,000 stochastic simulations (gray dots). In contrast, conditioning the transmission density on survival (black solid line) predicts the mean epidemic size over time reasonably well, and also equilibrates approximately at the correct level in stationarity. Overall though, there is large variation in the epidemic sizes between different trajectories, as shown by the broad light shaded region corresponding to the 90% inter-quantile range of the simulated trajectories. To model the number of secondary infections, we have used the Poisson distribution in the figure because the adjustment of the transmission rate does not result in explicit expressions for the negative binomial

medRxiv preprint doi: https://doi.org/10.1101/2020.11.17.20233403; this version posted June 7, 2021. The copyright holder for this preprint (which was not certified by peer review) is the author/funder, who has granted medRxiv a license to display the preprint in perpetuity. It is made available under a CC-BY 4.0 International license .

case. Cumulative epidemic sizes in case the number of secondary infections is distributed according to a negative binomial distribution show more variation due to the larger variance in the number of secondary infections (Fig. A in Appendix E).

4 Applications

We now apply the theoretical results obtained above. First, we use the approximation of the epidemic size (Eq. (11)) to estimate the probability distribution of the emergence time of the variant of concern B.1.1.7, first detected in the UK in September 2020. The distribution of the emergence time further provides insight into the probability distribution of the size of the cluster when the variant was first sampled. As a second application, we predict the success of mass testing, which has been applied by some regions and countries, e.g. Slovakia (Pavelka et al., 2021), during the COVID-19 pandemic to try to identify all infected individuals at a given moment. Last, we estimate the minimal testing frequency necessary to detect new emerging clusters before they exceed a certain size (on average). This prediction is especially relevant when the number of infected individuals is rare.

4.1 Distribution of the first detection time and cluster size at detection, and application to the origin of variant of concern B.1.1.7

The variant B.1.1.7, first detected in the UK from a sample that was collected on September 20th 2020 (Rambaut et al., 2020), has rapidly become a major variant of concern due to its increased transmissibility (Volz et al., 2021) and pathogenicity (Davies et al., 2021). Here, we develop a method to estimate the first infection of an individual with this variant and the distribution of the size of the B.1.1.7-cluster on the day when the sample was taken in September, based on the dynamics of the epidemic size of a local cluster.

Our analysis requires the effective reproduction number, estimated to be $R = 1.5$ for the variant B.1.1.7 in November 2020 in the UK (Volz et al., 2021), and the probability for a sample taken in the UK to be sequenced, which was around 4.2% in October 2020 (COVID-19 Genomics Consortium UK, 2020 – accessed February 9th, 2021). We will use this value in our analysis, keeping in mind that this might be an underestimate because the number of cases has been lower in September so the percentage of samples that could have been sequenced is potentially higher. Since only reported cases can be sampled, we additionally account for underreporting of cases. We assume that around 25% of all infections are detected (Colman et al., 2021). Lastly, we need to define a distribution for the time that passes between infection and sampling of an infectious individual. We assume that the time from infection to sampling is a gamma distributed random variable (but any distribution would work) with a mean of seven days and a standard deviation of two days. The parameter values (Table 1) are chosen such that they give a probability of sampling an infected individual up until 3 days of their infection that is less than 1%, and a probability of sampling an infected individual after ten days of their infection that is less than 10%. All parameters and probability distributions are summarized in Table 1.

Distribution of the first detection time

To estimate the time of the first detection of an individual infected by the strain B.1.1.7, we combine the sampling probability distribution f_{sampling} with the expected epidemic size at time t, given by the adjusted version of the epidemic size in Eq. (11), and the number of infections until the first infected in the cluster is sampled and sequenced, which happens with probability p_{sampling} per infected individual. In the following, for simplicity, we will refer to this first infected individual that is

medRxiv preprint doi: https://doi.org/10.1101/2020.11.17.20233403; this version posted June 7, 2021. The copyright holder for this preprint (which was not certified by peer review) is the author/funder, who has granted medRxiv a license to display the preprint in perpetuity. It is made available under a CC-BY 4.0 International license .

Interpretation	Distribution	Parameters	Reference
mean number of secondary infections	Poisson	$R = 1.5$	Volz et al. (2021)
time of secondary infection	Gamma (density: $\mu(t)$)	shape: 6.6, scale: 0.833 (mean: 5.5 days)	Github - OpenABM-Covid19 (Hinch et al., 2020)
time from infection to sampling	Gamma (density: $f_{\text{sampling}}(t)$)	shape: 12, scale: 7/12 (mean: 7 days)	–
sequencing probability	Bernoulli	$p_{\text{sequencing}} = 0.042$	COVID-19 Genomics Consortium UK (2020 – accessed February 9th, 2021)
sampling probability	Bernoulli	$p_{\text{sampling}} = 0.25 \times p_{\text{sequencing}}$	Colman et al. (2021)

Table 1: **Probability distributions and parameter values used in the case study of the variant B.1.1.7.**

sampled and sequenced by case X and also only write sampling when in fact we mean sampling and sequencing. The number of infection events till case X is infected, including case X, is denoted N_{inf}. It is a geometrically distributed number with probability p_{sampling}. That is, counting the infections until case X is infected resembles a discrete waiting process with 'success' probability p_{sampling}. Note that if we were interested in the jth sampling event, the number of infected individuals until the jth sampling event would be distributed according to a negative binomial distribution with success probability p_{sampling} and dispersion $\kappa = j$.

We now combine the distribution of N_{inf} with the *deterministic* time needed for the infected population to reach N_{inf} individuals (conditioned on non-extinction of this epidemic cluster as computed in Eq. (11)). We also refer to this time as *hitting time* and denote it by $t^{\text{det}}_{N_{\text{inf}}}$. Lastly, we add the probability density of the time from infection to sampling of case X to this deterministically computed time. Denoting by T_{sampling} the random time of first detection and sampling, its density is given by:

$$\begin{aligned} h_{\text{sampling}}(t) &:= \lim_{\text{dt}\to 0} \mathbf{P}\left(T_{\text{sampling}} \in (t-\text{dt}, t+\text{dt})\right) \\ &\approx \sum_{i=1}^{\infty} \mathbf{P}\left(N_{\text{inf}} = i\right)\ f_{\text{sampling}}\left(t - t_i^{\text{det}}\right) \\ &= \sum_{i=1}^{\infty} p_{\text{sampling}}\left(1 - p_{\text{sampling}}\right)^{i-1} f_{\text{sampling}}\left(t - t_i^{\text{det}}\right), \end{aligned} \tag{13}$$

where $f_{\text{sampling}}(s)$ denotes the probability density of the time from infection to sampling evaluated at time s (Table 1). It is important to keep in mind that the density of the first sampling time $h_{\text{sampling}}(t)$ is an approximation, because it is based on the mean epidemic size and not the whole distribution of the epidemic size. The mean epidemic size directly provides the deterministic hitting time t_i^{det}, neglecting the whole distribution of the epidemic size.

With our COVID-19-specific parameter set given in Table 1, we find that the mean time between the first infection of an individual with the variant B.1.1.7 and sampling of case X is around 46 days,

medRxiv preprint doi: https://doi.org/10.1101/2020.11.17.20233403; this version posted June 7, 2021. The copyright holder for this preprint (which was not certified by peer review) is the author/funder, who has granted medRxiv a license to display the preprint in perpetuity. It is made available under a CC-BY 4.0 International license .

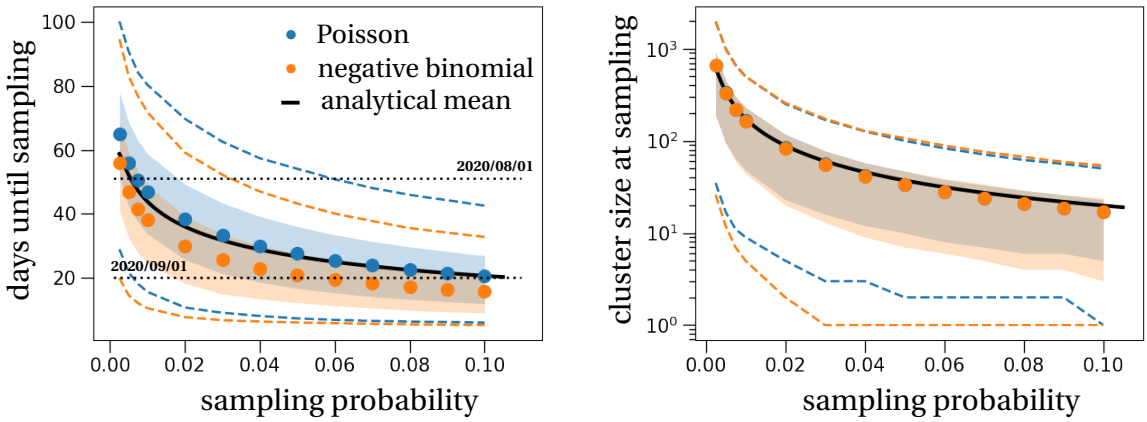

(a) first detection time

(b) cluster size at detection

Figure 3: **The date of emergence of the first infected with B.1.1.7 in the UK and the cluster size when varying the sampling probability.** The shaded regions and dashed lines show the 50% and 90% inter-quantile ranges obtained from 10,000 stochastic simulations that resulted in cluster establishment; blue for the secondary infections being Poisson distributed, orange for a negative binomial distribution. Dots represent the means of these simulations when varying the sampling probability. The effective reproduction number is set to $R = 1.5$, the dispersion parameter is $\kappa = 0.57$ (Salje et al., 2020), and the transmission density $\mu(t)$ and the waiting time between infection and sampling (f_{sampling}) are Gamma distributions with parameters as stated in Table 1. (a) The theoretical mean (black solid line) of the first sampling time is calculated from Eq. (13), which only applies to the Poisson case. (b) The mean cluster size of infected individuals with the variant B.1.1.7 at the first sampling time of this strain, i.e. the day the sample is taken, is calculated from Eq. (14).

indicating that the strain was present in the UK the 4th of August 2020 – yet, the variance is quite large for this distribution: the standard deviation is 19.5 days. Yet, the emergence date of the variant B.1.1.7 strongly depends on the sampling probability: smaller sampling probabilities result in earlier possible emergence dates than larger probabilities (Fig. 3a). The distribution of secondary cases also impacts the timing: if the number of secondary infections is distributed as a negative binomial distribution, the date of emergence shifts closer to the date of sampling of case X. This effect is secondary though, compared to the impact of the detection probability (Fig. 3a). Importantly, we also find that small increases in the sampling probability initially result in a large benefit when measured in the cluster sizes at the time of their detection (Fig. 3b). We discuss this observation in more detail in the section concerned with the minimal testing frequency.

In general, we find that the theoretical prediction of the probability distribution of the first sampling time fits the stochastic simulation results well (Fig. 4a). Note that this implies that most of the variability in time does not come from stochasticity in epidemic size, but from variability in the timing of detection. However, we find the largest discrepancy between theory and simulations at large first sampling times, i.e., we underestimate the right tail of the first sampling time distribution. This difference arises because our theoretical approximation does not take into account variability in the epidemic size process. Fig. 2 shows a large variation in the number of infected individuals over time between different stochastic trajectories. Most notably, there are several trajectories that remain at low cumulative epidemic sizes for a relatively long time. In particular, these trajectories are responsible

medRxiv preprint doi: https://doi.org/10.1101/2020.11.17.20233403; this version posted June 7, 2021. The copyright holder for this preprint (which was not certified by peer review) is the author/funder, who has granted medRxiv a license to display the preprint in perpetuity. It is made available under a CC-BY 4.0 International license .

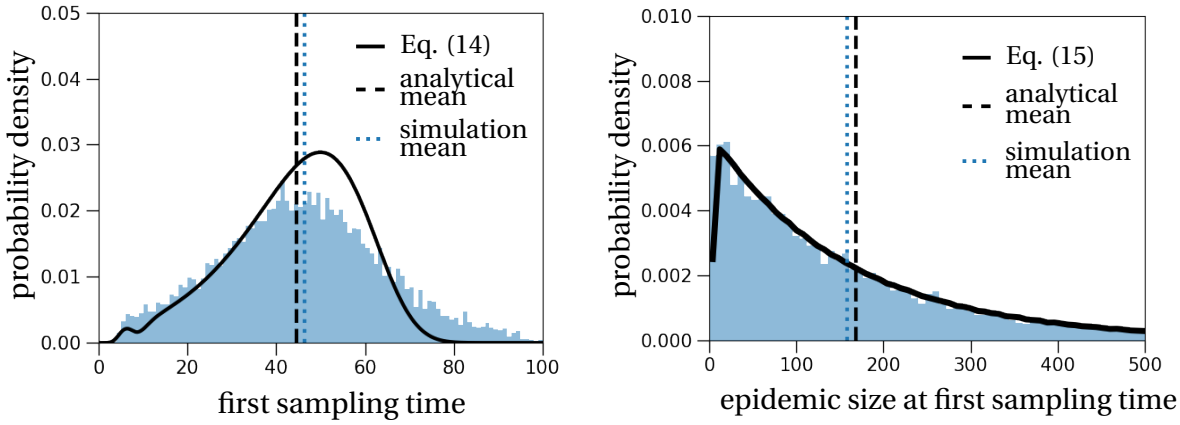

(a) first sampling time

(b) cluster size at first sampling

Figure 4: **Distribution of the first sampling time and the cluster size at that time, parameterized to the case of the variant B.1.1.7.** The histograms are obtained from 10,000 stochastic simulations and represent (a) the time since first infection (in days) and (b) the cluster size at this time. The theoretical predictions (black solid lines) are computed by Eqs. (13) and (14). The cumulative epidemic size is computed by Eq. (11), the process conditioned on establishment of an infection cluster. The parameters and distributions are as stated in Table 1.

for the long right tail of the sampling time distribution in Fig. 4a.

Cluster size at the first detection time

In a next step, we use this distribution of the first sampling time to infer the size of the epidemic cluster at that random time. Therefore, we combine the adjusted epidemic size in Eq. (11) with Eq. (13) and obtain the following probability mass function for the size of the cluster at the sampling time of case X:

$$\mathbf{P}\left(I(T_{\text{sampling}}) = k\right) = \int_0^\infty h_{\text{sampling}}(t)\mathbb{1}_{\{\tilde{I}(t)\in[k-1/2,k+1/2)\}}\,dt\,. \tag{14}$$

This estimate of the epidemic size distribution approximates the simulated data reasonably well (Fig. 4b). The only notable difference occurs for very low epidemic sizes, where the epidemic size at the first sampling time ranges from 0-8 (bin size is set to 8 – the smallest bin size that produces continuous theoretical prediction), as can be seen in the histogram in Fig. 4b. The mean size of the cluster with the variant B.1.1.7 at the first sampling time (obtained from the stochastic simulations) consists of 159 individuals, yet again with a large standard deviation of 158 individuals. For example, the 95-percentile of the simulations predicts a cluster size of 476 infected individuals with the variant B.1.1.7 by the time of the first sampling of the variant.

As expected, when varying the detection probability, the mean size of the cluster at detection follows the exponential growth curve of the cumulative epidemic size: the higher the probability density, the lower the average size of the cluster at its detection (Fig. 3b). Additionally, we find that the type of probability distribution for the number of secondary infections (negative binomial or Poisson), does not affect the mean of the cluster size. Similarly, the variance of the cluster size at detection, as obtained from 10,000 stochastic simulations, does not vary strongly between the two distributions of secondary infections.

medRxiv preprint doi: https://doi.org/10.1101/2020.11.17.20233403; this version posted June 7, 2021. The copyright holder for this preprint (which was not certified by peer review) is the author/funder, who has granted medRxiv a license to display the preprint in perpetuity. It is made available under a CC-BY 4.0 International license .

4.2 Detection rate of a single mass testing effort

A good measure to evaluate the prevalence of the disease in the population is the number of detected cases, which depends on the testing effort. In the context of COVID-19, the average detection rate on the 8th of May 2020 across a large number of countries, mainly in Europe and North America, was inferred to be around 30% at best (Belloir and Blanquart, 2021; Russell et al., 2020). However, test capacity is not the only limiting factor to detect infected individuals. The probability for an infected individual to test positive by a reverse polymerase chain reaction or a lateral flow test (LFT), which we will more loosely refer to as rapid tests, varies over the course of the individual's infection (Kucirka et al., 2020; Borremans et al., 2020; Hellewell et al., 2021). Here, we will use the data obtained for rapid tests in Hellewell et al. (2021, Fig. 4B) and for reverse transcriptase polymerase chain reaction (RT-PCR) tests in Kucirka et al. (2020, Fig. 2), as plotted in Fig. 5a. During the first three days of an infection, the viral load within the infected individual is too low to reliably detect the virus with both testing procedures. The probability of detection then reaches a maximum around day four post-infection and then gradually declines. The decline is much faster for rapid tests than for RT-PCR tests. In the following, we denote the probability to test positive on day a after infection by $Q(a)$.

Using the probabilities for testing positive by a rapid test and an RT-PCR test (Fig. 5a), we compute an upper bound for the fraction of detectable infectious individuals within the epidemic outbreak.Note that this result does not rely on our stochastic correction of the deterministic dynamics, nor does it depend on the epidemic size over time. Instead, the result only depends on the stationary infection age distribution, which is determined by the Malthusian growth rate r. Therefore, this result is true for any exponentially growing epidemic.

Again using general branching processes theory (Jagers, 1969; Haccou et al., 2005), we find that the number of detectable individuals in the population at time t is given as a fraction q of the overall epidemic size as given in Eq. (11). The fraction q is defined as

$$q = \frac{1}{C} \int_0^T Q(a) r e^{-ra} da, \tag{15}$$

where $C = \int_0^T r e^{-ra} da = 1 - e^{-Tr}$ is the proportion of individuals that have been infected less than T days ago. The integral in Eq. (15) computes the fraction of individuals that are detectable (term $Q(a)$ integrated over the stationary infection age distribution (term re^{-ra}) of the population, restricted to the age of infection being less than T days (constant C). For the numerical example, we assume that after $T = 14$ days infected individuals are not infectious anymore. The resulting truncated distributions for $R = 2.9$ and $R = 1.3$ are plotted in Fig. 5a.

With a high reproduction number $R = 2.9$, we find $q \approx 0.255$ (evaluating a discretized version of the integral) when testing is done by rapid tests, so that we would expect that only about 25.5% of the infected individuals would test positive with a rapid test at each point in time. Using the RT-PCR data instead, we find $q = 0.29$. These estimates strongly depend on the combination of the probability to test positive $Q(a)$ and the stationary infection age distribution. The stationary infection age distribution itself depends on the Malthusian growth rate r (Eq. (7)). If we reduce the reproduction number to $R = 1.3$, the detection rates become $q = 0.265$ and $q = 0.48$ for rapid tests and RT-PCR tests, respectively. Interestingly, the fraction of detectable cases does not change in the rapid test scenario substantially, which is a robust result for all possible reproduction numbers between 1.1 and 3. This seems to be due to our choice to only consider individuals with an age of infection less than 14 days. For other choices of this infectiousness threshold, the difference between the detection rates for the two reproduction numbers is more notable. In case of the RT-PCR test, the detection rate increased a lot with a lower reproduction number, from 29% for $R = 2.9$ to 48% for $R = 1.3$. The explanation for this increase in detection rate is that in slowly growing epidemics, more individuals are infected a long

medRxiv preprint doi: https://doi.org/10.1101/2020.11.17.20233403; this version posted June 7, 2021. The copyright holder for this preprint (which was not certified by peer review) is the author/funder, who has granted medRxiv a license to display the preprint in perpetuity. It is made available under a CC-BY 4.0 International license .

time ago and remain detectable with RT-PCR, whereas in faster growing epidemics many individuals are not yet detectable because they were infected within the last two days.

4.3 Minimal testing frequency to detect clusters of a certain size

Given that a single mass testing effort does not provide a large detection rate of potentially infectious individuals, we now ask whether repeated random testing in the population is a more feasible strategy to contain an infection cluster. Specifically, how often should we randomly test the population to detect a cluster before it exceeds a certain size? As a numerical example we will use a threshold cluster size of 30 infected individuals. We assume that testing is applied population-wide at random, independently of the infection state of an individual. As pointed out above, the probability to test positive depends on the age of infection of an individual (Borremans et al., 2020; Kucirka et al., 2020; Hellewell et al., 2021).

If a fraction f of the population is tested every day, the detection probability of an infected individual is approximately given by

$$p_{\text{detect}} = 1 - \prod_{a=1}^{\infty} (1 - fQ(a)) \approx f \sum_{a=1}^{\infty} Q(a) \tag{16}$$

The term $(1 - fQ(a))$ is the probability that an infected individual is not detected at age of infection a. Hence, the product is the probability that an individual is never detected over the course of the individual's infection. The probability of detection is one minus this product. The approximation is valid when it is very unlikely that the same individual is tested more than once during the period when there is a high chance to detect their infection.

To determine the testing frequency above which the expected cluster size is smaller than 30 infected individuals, we repeat the steps from the previous sections: first, we determine the first detection time and then translate this result to the average cluster size at detection. Since our analytical result tends to overestimate the cluster size at detection (Fig. 5b), this analytical procedure will provide an upper bound for the true testing frequency required to detect clusters of a certain size. In our numerical example with $R = 1.1$, this procedure results in a testing frequency of 0.013 for a threshold cluster size of 30 infected individuals. In reality, as obtained from the simulations, this testing frequency even detects clusters with on average 20 infected individuals at the time of detection (Fig. 5).

Fig. 5b also shows that the epidemic size at detection reflects the exponential growth of the epidemic. Increasing the testing frequency when it is still low offers large benefits in terms of cluster size at detection. Thus, there might be a clear optimal testing frequency that ensures clusters are relatively small when detected while not overwhelming test systems.

5 Discussion

We have collected key equations and derived novel results to account for stochasticity during the early phase of epidemic trajectories. Explicitly taking into account stochastic effects during the early phase of an epidemic allowed us to compute a good description of the mean epidemic size for all times (Eq. (11)). Importantly, our result captures the increased initial growth rate of surviving epidemics when compared to the asymptotic growth rate (Fig. 2). This is a known effect (Mercer et al., 2011; Rebuli et al., 2018), yet cannot be captured by deterministic epidemiological compartment models or by the McKendrick-von Foerster equation. One important consequence of this theoretical underestimation of classically used models is that parameter inference during the early phase of an epidemic of, for example, the basic reproduction number, will result in an overestimation of the true value (Kochańczyk et al., 2020). We provide a new mathematical description of the expected epidemic size over time that could be used in statistical inference during the early phase of emerging epidemics.

medRxiv preprint doi: https://doi.org/10.1101/2020.11.17.20233403; this version posted June 7, 2021. The copyright holder for this preprint (which was not certified by peer review) is the author/funder, who has granted medRxiv a license to display the preprint in perpetuity. It is made available under a CC-BY 4.0 International license .

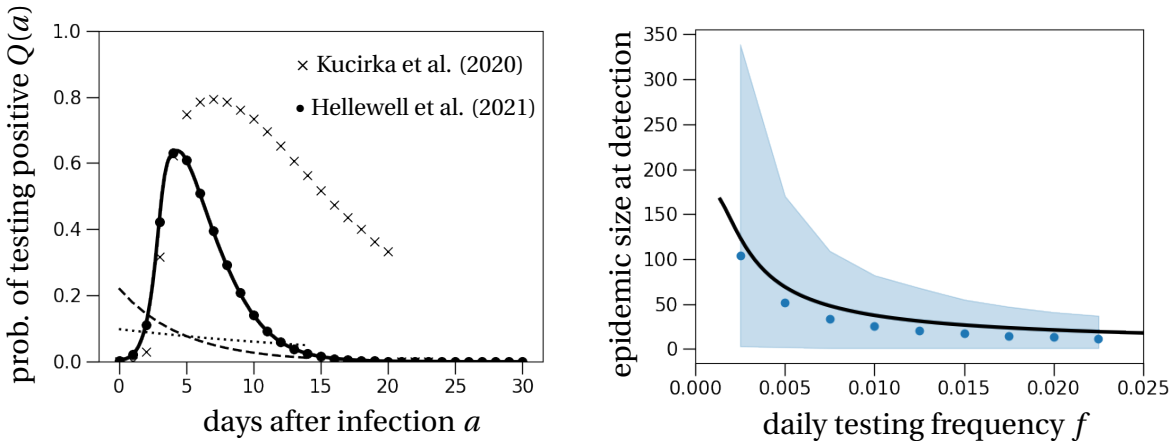

(a) Probability of testing positive

(b) Cluster size vs. fraction of daily tests

Figure 5: **Average epidemic cluster size at detection depending on the daily testing frequency.** (a) The probability for an infected individual to test positive by a rapid test (bullet points) and a RT-PCR test (crosses) is close to zero during the first two days after infection. It then increases up to approximately 0.6 on day 4 after infection for rapid tests and up to 0.8 on day 8 for RT-PCR tests. The probability of testing positive then decreases. For rapid tests, the probability of testing positive approaches zero by day 21 after infection. For the RT-PCR test, the probability of testing positive remains relatively high at least until day 20, which corresponds to the last estimated time point in Fig. 2 (upper panel) from Kucirka et al. (2020). The probabilities for rapid tests are based on data from Fig. 4B in Hellewell et al. (2021). The dashed and dotted lines show the re-normalized stationary infection age distributions for $R = 2.9$ and $R = 1.3$ (Eq. (15)). (b) The shaded region shows the 90% confidence interval of the cluster size obtained from 10,000 stochastic simulations that resulted in cluster establishment. Dots represent the average cluster sizes of these simulations at the first detection time. The theoretical prediction (black solid line) is obtained from Eq. (14), adapted to the setting of testing. In particular, the distribution until detection is motivated by the probability to test positive in Fig. 5a and translated to a detection probability by Eq. (16). The effective reproduction number is set to $R = 1.1$ and the number of secondary infections is Poisson-distributed. The transmission density $\mu(t)$ is as stated in Table 1.

In a next step, we then applied our new theoretical result on the mean epidemic size over time to public health relevant questions.

As a first application, we analytically derived the probability distribution of the first detection time of an epidemic cluster. While in principle applicable to any type of detection event, as for instance the first death or the first hospitalization event, we have focused on dating the emergence of the variant B.1.1.7 that was first sampled in the UK the 20th of September 2020. Our methodology results in a cluster age of 46 days on average, which means that the variant was likely present in the UK the 4th of August 2020. Usually, phylogenetic or phylodynamic methods are used to date the evolutionary history of mutations (e.g Hadfield et al., 2018). In this particular case, this approach fails because of an excess number of mutations in the B.1.1.7 lineage when compared to strains sampled at a similar time (Rambaut et al., 2020), so that the typical molecular clock approach is not applicable. In addition, we derived an analytical approximation for the probability distribution of the epidemic size at the first detection event. In contrast to a previous numerical estimate of the cluster size at the

medRxiv preprint doi: https://doi.org/10.1101/2020.11.17.20233403; this version posted June 7, 2021. The copyright holder for this preprint (which was not certified by peer review) is the author/funder, who has granted medRxiv a license to display the preprint in perpetuity. It is made available under a CC-BY 4.0 International license .

first disease-caused death that relies solely on the waiting time distribution until detection, e.g. the distribution from infection to death (Jombart et al., 2020), we consider the whole epidemic trajectory of the cluster, i.e., from the first infected individual to the day of detection. The previously proposed method inevitably results in an overestimate of the actual epidemic size. Previous research has also shown that if the probability of detection since infection were constant over time, which is not the case in our examples above, the cluster size at detection would be geometrically distributed (Trapman and Bootsma, 2009; Lambert and Trapman, 2013). Whether the distribution of cluster sizes at detection is a geometric distribution if the detection process is not constant in time, is an open question. In our specific data set, this seems to be the case (Fig. 4b).

We also applied our results to the evaluation of testing strategies. Currently, aside from vaccination campaigns, frequent testing is seen as a possible solution to relax COVID-19-related restrictions in the short term. Our modeling approach gives an estimation of the minimal testing frequency per day to detect epidemic clusters of a certain size, for example small enough for manual contact tracing to be possible. The minimal testing frequency depends on the test that is employed. In our numerical example, we have used the detection probability estimated for rapid tests, which were collected during the early phase of the epidemic in the UK in 2020 (Hellewell et al., 2021). Since then, tests have improved so that our estimation of the minimal testing frequency is very likely an overestimate. We find that for a cluster size to be below 30 infected individuals (on average), each day around 0.13% of a total population would need to be randomly selected for testing, i.e., independently of the individual's infection status. For example, with the French population size, this would translate to 871,000 daily tests. Pooled sample testing strategies could be a solution to reduce the number of testing kits needed, and is a particularly reasonable option when the positive testing rate is very low (Brault et al., 2021), i.e., when the prevalence of infected individuals in a community is close to zero.

We also estimated the fraction of cases that can be detected during a single mass testing efforts, as has been for example implemented in Slovakia in fall 2020 (Pavelka et al., 2021). This estimated detection rate is valid for any exponentially growing epidemic, i.e. when the number of susceptible individuals is not limiting. We emphasize that it is estimated using the deterministic component of our model, and is therefore valid for large outbreak sizes, and less so in the early phase of an outbreak. The detection rate in this situation depends solely on the stationary distribution of the age of infection, which again depends on the exponential growth rate r that is derived from the transmission density μ and the effective reproduction number R (Eq. (7)). With both $R = 1.3$ and $R = 2.9$, we find that only about 26% of potentially infectious individuals would test positive, based on the detection capacity of rapid tests as reported in Hellewell et al. (2021). As already stated above, this percentage is most likely an underestimate due to improved test sensitivity. Using the probabilities to test positive by an RT-PCR test (Kucirka et al., 2020), the detection rates are 48% and 29% for reproduction numbers $R = 1.3$ and $R = 2.9$. With both testing strategies though, a certain fraction of individuals that is not detected is still in the latent phase of the infection (0-3 days post-infection) and will become infectious after the mass testing event. In our numerical example with $R = 1.3$, this fraction corresponds to approximately 28% of all potentially infectious individuals (age of infection smaller than 14 days) in the total epidemic outbreak. For $R = 2.9$, this fraction increases to even 50%. Similar observations have also been made by employing a deterministic SEIR-model (Bosetti et al., 2021). This result indicates that only isolating positively detected individuals would be insufficient to contain the epidemic and that mass testing would need to be repeated to efficiently control the epidemic.

In conclusion, we have summarized existing theoretical results describing the early, stochastic dynamics of an epidemic, and we have developed new results on the mean epidemic size trajectory. We have outlined how to compute the establishment probability and combined it with the deterministic McKendrick-von Foerster equation to obtain a precise description of the expected epidemic size of

medRxiv preprint doi: https://doi.org/10.1101/2020.11.17.20233403; this version posted June 7, 2021. The copyright holder for this preprint (which was not certified by peer review) is the author/funder, who has granted medRxiv a license to display the preprint in perpetuity. It is made available under a CC-BY 4.0 International license .

an establishing epidemic over time. As an application, we approximated the probability distribution for the timing of a first infected individual in an epidemic cluster. This distribution can be used to estimate, for example, the emergence of new variants of a pathogen, like the SARS-CoV-2 variant of concern B.1.1.7. In addition, we derived analytical approximations on the effect of mass testing and the minimal testing frequency to detect clusters below a certain size. These applications are relevant from a public health perspective and could be used to guide the policy to contain and fight any infectious disease.

Data availability

The C++ codes, data files and Python scripts used to generate the figures are available at `https://gitlab.com/pczuppon/early-epidemic-dynamics`.

Acknowledgements

PC has received funding from the European Union's Horizon 2020 research and innovation program under the Marie Skłodowska-Curie grant agreement PolyPath 844369. FD is funded by an Agence Nationale de la Recherche JCJC grant TheoGeneDrive ANR-19-CE45-0009-01. FB is funded by a Momentum grant from the CNRS.

References

Athreya, K. B. and Ney, P. E. *Branching Processes*. Springer Berlin Heidelberg, 1972. doi: 10.1007/978-3-642-65371-1.

Belloir, A. and Blanquart, F. Estimating the global reduction in transmission and rise in detection capacity of the novel coronavirus SARS-CoV-2 in early 2020. *Epidemics*, 35:100445, 2021. doi: 10.1016/j.epidem.2021.100445.

Borremans, B., Gamble, A., Prager, K., Helman, S. K., McClain, A. M., Cox, C., Savage, V., and Lloyd-Smith, J. O. Quantifying antibody kinetics and RNA detection during early-phase SARS-CoV-2 infection by time since symptom onset. *eLife*, 9, 2020. doi: 10.7554/elife.60122.

Bosetti, P., Kiem, C. T., Yazdanpanah, Y., Fontanet, A., Lina, B., Colizza, V., and Cauchemez, S. Impact of mass testing during an epidemic rebound of SARS-CoV-2: a modelling study using the example of France. *Eurosurveillance*, 26(1), 2021. doi: 10.2807/1560-7917.es.2020.26.1.2001978.

Brault, V., Mallein, B., and Rupprecht, J.-F. Group testing as a strategy for COVID-19 epidemiological monitoring and community surveillance. *PLOS Computational Biology*, 17(3):e1008726, 2021. doi: 10.1371/journal.pcbi.1008726.

Britton, T. and Tomba, G. S. Estimation in emerging epidemics: biases and remedies. *Journal of The Royal Society Interface*, 16(150):20180670, 2019. doi: 10.1098/rsif.2018.0670.

Chetrite, R. and Touchette, H. Nonequilibrium markov processes conditioned on large deviations. *Annales Henri Poincaré*, 16(9):2005–2057, 2015. doi: 10.1007/s00023-014-0375-8.

Cohn, H. A martingale approach to supercritical (CMJ) branching processes. *The Annals of Probability*, 13(4), 1985. doi: 10.1214/aop/1176992803.

medRxiv preprint doi: https://doi.org/10.1101/2020.11.17.20233403; this version posted June 7, 2021. The copyright holder for this preprint (which was not certified by peer review) is the author/funder, who has granted medRxiv a license to display the preprint in perpetuity. It is made available under a CC-BY 4.0 International license .

Colman, E., Enright, J., Puspitarani, G. A., and Kao, R. R. Estimating the proportion of SARS-CoV-2 infections reported through diagnostic testing. *medRxiv preprint*, 2021. doi: 10.1101/2021.02.09.21251411.

COVID-19 Genomics Consortium UK. *How do we collect and sequence SARS-CoV-2 samples?*, 2020 – accessed February 9th, 2021. URL `https://www.cogconsortium.uk/news_item/how-do-we-collect-and-sequence-sars-cov-2-samples/`.

Crump, K. S. and Mode, C. J. A general age-dependent branching process. I. *Journal of Mathematical Analysis and Applications*, 24(3):494–508, 1968. doi: 10.1016/0022-247x(68)90005-x.

Crump, K. S. and Mode, C. J. A general age-dependent branching process. II. *Journal of Mathematical Analysis and Applications*, 25(1):8–17, 1969. doi: 10.1016/0022-247x(69)90210-8.

Davies, N. G., Abbott, S., Barnard, R. C., Jarvis, C. I., Kucharski, A. J., Munday, J. D., Pearson, C. A. B., Russell, T. W., Tully, D. C., Washburne, A. D., Wenseleers, T., Gimma, A., Waites, W., Wong, K. L. M., van Zandvoort, K., Silverman, J. D., CMMID COVID-19 Working Group, COVID-19 Genomics UK (COG-UK) Consortium, Diaz-Ordaz, K., Keogh, R., Eggo, R. M., Funk, S., Jit, M., Atkins, K. E., and Edmunds, W. J. Estimated transmissibility and impact of SARS-CoV-2 lineage B.1.1.7 in England. *Science*, 372(6538):eabg3055, 2021. doi: 10.1126/science.abg3055.

Diekmann, O. and Heesterbeek, J. *Mathematical epidemiology of infectious diseases: model building, analysis and interpretation*. Wiley series in mathematical and computational biology. John Wiley and Sons, United States, 2000. ISBN 9780471986829.

Doob, J. Conditional brownian motion and the boundary limits of harmonic functions. *Bulletin de la Société Mathématique de France*, 79:431–458, 1957. doi: 10.24033/bsmf.1494.

Endo, A., Abbott, S., Kucharski, A. J., and Funk, S. Estimating the overdispersion in COVID-19 transmission using outbreak sizes outside China. *Wellcome Open Research*, 5:67, 2020. doi: 10.12688/wellcomeopenres.15842.3.

Ethier, S. N. and Kurtz, T. G. *Markov processes: characterization and convergence*. Wiley series in probability and mathematical statistics. J. Wiley & Sons, New York, Chichester, 1986.

Forien, R., Pang, G., and Pardoux, É. Estimating the state of the COVID-19 epidemic in France using a model with memory. *Royal Society Open Science*, 8(3), 2021. doi: 10.1098/rsos.202327.

Foutel-Rodier, F., Blanquart, F., Courau, P., Czuppon, P., Duchamps, J.-J., Gamblin, J., Kerdoncuff, É., Kulathinal, R., Régnier, L., Vuduc, L., Lambert, A., and Schertzer, E. From individual-based epidemic models to McKendrick-von Foerster PDEs: A guide to modeling and inferring COVID-19 dynamics. *arXiv preprint*, 2020.

Gatto, M., Bertuzzo, E., Mari, L., Miccoli, S., Carraro, L., Casagrandi, R., and Rinaldo, A. Spread and dynamics of the COVID-19 epidemic in italy: Effects of emergency containment measures. *Proceedings of the National Academy of Sciences*, 117(19):10484–10491, 2020. doi: 10.1073/pnas.2004978117.

Haccou, P., Jagers, P., and Vatutin, V. A. *Branching Processes*. Cambridge University Press, 2005. doi: 10.1017/cbo9780511629136.

medRxiv preprint doi: https://doi.org/10.1101/2020.11.17.20233403; this version posted June 7, 2021. The copyright holder for this preprint (which was not certified by peer review) is the author/funder, who has granted medRxiv a license to display the preprint in perpetuity. It is made available under a CC-BY 4.0 International license .

Hadfield, J., Megill, C., Bell, S. M., Huddleston, J., Potter, B., Callender, C., Sagulenko, P., Bedford, T., and Neher, R. A. Nextstrain: real-time tracking of pathogen evolution. *Bioinformatics*, 34(23): 4121–4123, 2018. doi: 10.1093/bioinformatics/bty407.

Hellewell, J., , Russell, T. W., Beale, R., Kelly, G., Houlihan, C., Nastouli, E., Kucharski, A. J., and and. Estimating the effectiveness of routine asymptomatic PCR testing at different frequencies for the detection of SARS-CoV-2 infections. *BMC Medicine*, 19(1), 2021. doi: 10.1186/s12916-021-01982-x.

Hinch, R., Probert, W. J. M., Nurtay, A., Kendall, M., Wymatt, C., Hall, M., Lythgoe, K., Cruz, A. B., Zhao, L., Stewart, A., Ferretti, L., Montero, D., Warren, J., Mather, N., Abueg, M., Wu, N., Finkelstein, A., Bonsall, D. G., Abeler-Dorner, L., and Fraser, C. OpenABM-covid19 - an agent-based model for non-pharmaceutical interventions against COVID-19 including contact tracing. *medRXiv preprint*, 2020. doi: 10.1101/2020.09.16.20195925.

Jagers, P. A general stochastic model for population development. *Scandinavian Actuarial Journal*, 1969(1-2):84–103, 1969. doi: 10.1080/03461238.1969.10405220.

Jombart, T., van Zandvoort, K., Russell, T. W., Jarvis, C. I., Gimma, A., Abbott, S., Clifford, S., Funk, S., Gibbs, H., Liu, Y., Pearson, C. A. B., Bosse, N. I., Eggo, R. M., Kucharski, A. J., and Edmunds, W. J. Inferring the number of COVID-19 cases from recently reported deaths. *Wellcome Open Research*, 5: 78, 2020. doi: 10.12688/wellcomeopenres.15786.1.

Kochańczyk, M., Grabowski, F., and Lipniacki, T. Super-spreading events initiated the exponential growth phase of COVID-19 with $\mathscr{R}0$ higher than initially estimated. *Royal Society Open Science*, 7(9): 200786, 2020. doi: 10.1098/rsos.200786.

Kucirka, L. M., Lauer, S. A., Laeyendecker, O., Boon, D., and Lessler, J. Variation in false-negative rate of reverse transcriptase polymerase chain reaction–based SARS-CoV-2 tests by time since exposure. *Annals of Internal Medicine*, 173(4):262–267, 2020. doi: 10.7326/m20-1495.

Lambert, A. and Trapman, P. Splitting trees stopped when the first clock rings and vervaat's transformation. *Journal of Applied Probability*, 50(1):208–227, 2013. doi: 10.1239/jap/1363784434.

Linton, N., Kobayashi, T., Yang, Y., Hayashi, K., Akhmetzhanov, A., Jung, S., Yuan, B., Kinoshita, R., and Nishiura, H. Incubation period and other epidemiological characteristics of 2019 novel coronavirus infections with right truncation: A statistical analysis of publicly available case data. *Journal of Clinical Medicine*, 9(2):538, 2020. doi: 10.3390/jcm9020538.

Lloyd-Smith, J., Schreiber, S., Kopp, P., and Getz, W. Superspreading and the effect of individual variation on disease emergence. *Nature*, 438(7066):355–359, 2005. doi: 10.1038/nature04153.

McKendrick, A. G. Applications of mathematics to medical problems. *Proceedings of the Edinburgh Mathematical Society*, 44:98–130, 1925. doi: 10.1017/s0013091500034428.

Mercer, G. N., Glass, K., and Becker, N. G. Effective reproduction numbers are commonly overestimated early in a disease outbreak. *Statistics in Medicine*, 30(9):984–994, 2011. doi: 10.1002/sim.4174.

Pavelka, M., Van-Zandvoort, K., Abbott, S., Sherratt, K., Majdan, M., CMMID COVID-19 working group, Inštitút Zdravotných Analýz, Jarčuška, P., Krajčí, M., Flasche, S., and Funk, S. The impact of population-wide rapid antigen testing on SARS-CoV-2 prevalence in Slovakia. *Science*, 372(6542): 635–641, 2021. doi: 10.1126/science.abf9648.

medRxiv preprint doi: https://doi.org/10.1101/2020.11.17.20233403; this version posted June 7, 2021. The copyright holder for this preprint (which was not certified by peer review) is the author/funder, who has granted medRxiv a license to display the preprint in perpetuity. It is made available under a CC-BY 4.0 International license .

Rambaut, A., Loman, N., Pybus, O., Barclay, W., Barrett, J., Carabelli, A., Connor, T., Peacock, T., Robertson, D. L., Volz, E., and COVID-19 Genomics Consortium UK (CoG-UK)9. *Preliminary genomic characterisation of an emergent SARS-CoV-2 lineage in the UK defined by a novel set of spike mutations*, 2020. URL `https://bit.ly/3sBZ5Y4`.

Rebuli, N. P., Bean, N., and Ross, J. Estimating the basic reproductive number during the early stages of an emerging epidemic. *Theoretical Population Biology*, 119:26–36, 2018. doi: 10.1016/j.tpb.2017.10.004.

Russell, T. W., Golding, N., Abbott, S., Hellewell, J., Pearson, C. A. B., van Zandvoort, K., Jarvis, C. I., Gibbs, H., Liu, Y., Eggo, R. M., Edmunds, J. W., and Kucharski, A. J. Reconstructing the global dynamics of under-ascertained COVID-19 cases and infections. *medRXiv preprint*, 2020. doi: 10.1101/2020.07.07.20148460.

Salje, H., Tran Kiem, C., Lefrancq, N., Courtejoie, N., Bosetti, P., Paireau, J., Andronico, A., Hozé, N., Richet, J., Dubost, C.-L., Le Strat, Y., Lessler, J., Levy-Bruhl, D., Fontanet, A., Opatowski, L., Boëlle, P.-Y., and Cauchemez, S. Estimating the burden of SARS-CoV-2 in France. *Science*, 2020. doi: 10.1126/science.abc3517.

Svensson, Å. A note on generation times in epidemic models. *Mathematical Biosciences*, 208(1): 300–311, 2007. doi: 10.1016/j.mbs.2006.10.010.

Trapman, P. and Bootsma, M. C. J. A useful relationship between epidemiology and queueing theory: The distribution of the number of infectives at the moment of the first detection. *Mathematical Biosciences*, 219(1):15–22, 2009. doi: 10.1016/j.mbs.2009.02.001.

Volz, E., Mishra, S., Chand, M., Barrett, J. C., Johnson, R., Geidelberg, L., Hinsley, W. R., Laydon, D. J., Dabrera, G., O'Toole, Á., Amato, R., Ragonnet-Cronin, M., Harrison, I., Jackson, B., Ariani, C. V., Boyd, O., Loman, N. J., McCrone, J. T., Gonçalves, S., Jorgensen, D., Myers, R., Hill, V., Jackson, D. K., Gaythorpe, K., Groves, N., Sillitoe, J., Kwiatkowski, D. P., Flaxman, S., Ratmann, O., Bhatt, S., Hopkins, S., Gandy, A., Rambaut, A., and and, N. M. F. Transmission of SARS-CoV-2 lineage B.1.1.7 in England: Insights from linking epidemiological and genetic data. *medRxiv preprint*, 2021. doi: 10.1101/2020.12.30.20249034.

Wallinga, J. and Lipsitch, M. How generation intervals shape the relationship between growth rates and reproductive numbers. *Proceedings of the Royal Society B: Biological Sciences*, 274(1609):599–604, 2006. doi: 10.1098/rspb.2006.3754.

medRxiv preprint doi: https://doi.org/10.1101/2020.11.17.20233403; this version posted June 7, 2021. The copyright holder for this preprint (which was not certified by peer review) is the author/funder, who has granted medRxiv a license to display the preprint in perpetuity. It is made available under a CC-BY 4.0 International license .

A Infection age dependent probability of extinction

In this section, we compute the extinction probability of the epidemic when started with a single infected individual with age of infection a. In the main text, we have only considered the special case $a = 0$.

We consider a branching process approximation of the epidemic. We assume that each individual is characterized by its age of infection and we set $\tau(a)$ as the mean infectiousness at age a, i.e.,

$$\tau(a)da \;=\; \mathbf{P}(\text{individual with age of infection in } [a, a+da] \text{ infects a new individual}). \tag{A.1}$$

For $a > 0$, let $p_{\text{ext}}(a)$ be the probability that the epidemic starting with a single individual with age of infection a does not establish (in the main text we have computed $p_{\text{ext}}(0)$). More formally, if Z_t denotes the number of individuals infected at time t, then

$$p_{\text{ext}}(a) \;=\; \mathbf{P}_a\Big(\limsup Z_t < \infty\Big) = \sum_{k=0}^{\infty} p_{\text{ext}}(0)^k \mathbf{P}(Y_a = k), \tag{A.2}$$

where $\mathbf{P}_a$ is the probability distribution of the branching process starting from a single individual with age a and Y_a denotes the number of future secondary infections of an individual with age a. From this, in the case of a Poisson-distributed number of secondary infections, we find

$$\frac{d}{da} p_{\text{ext}}(a) \;=\; \tau(a)\big(1 - p_{\text{ext}}(0)\big)\, p_{\text{ext}}(a). \tag{A.3}$$

As a consequence

$$p_{\text{ext}}(a) \;=\; p_{\text{ext}}(0) \exp\Big((1 - p_{\text{ext}}(0)) \int_0^a \tau(s)ds\Big), \tag{A.4}$$

where $p_{\text{ext}}(0)$ can be determined by the boundary condition

$$\lim_{a\to\infty} p_{\text{ext}}(a) = 1\,, \tag{A.5}$$

which is ensured by the fact that $R < \infty$. (Intuitively, an individual infected a long time ago is not infectious anymore.) We then find $p_{\text{ext}}(0)$ as the unique solution of

$$p_{\text{ext}}(0) \exp\Big((1 - p_{\text{ext}}(0))R\Big) = 1, \text{ where } p_{\text{ext}}(0) < 1. \tag{A.6}$$

Note that the expression of $p_{\text{ext}}(0)$ is the same as the one stated in Section 2 in the main text in the case of a Poisson-distributed number of secondary infections.

medRxiv preprint doi: https://doi.org/10.1101/2020.11.17.20233403; this version posted June 7, 2021. The copyright holder for this preprint (which was not certified by peer review) is the author/funder, who has granted medRxiv a license to display the preprint in perpetuity. It is made available under a CC-BY 4.0 International license .

B Derivation of the asymptotic limit

We consider a Crump-Mode-Jagers process, also referred to as a general branching process, with an unspecified distribution of secondary infections to model the number of infected individuals over time. The random variable for the number of secondary infections is denoted by Y. We define τ as the intensity measure of the process, i.e., such that for every test function f

$$\mathbf{E}\left[\sum_{i=1}^{Y} f(t_i)\right] = \int_0^\infty f(u)\tau(u)du \tag{B.1}$$

and the correlation intensity measure c such that

$$\mathbf{E}\left[\mathbb{1}_{Y\geq 2}\sum_{i\neq j} f(t_i,t_j)\right] = \int_0^\infty f(u,v)c(u,v)dudv. \tag{B.2}$$

We assume the Kesten-Stigum condition

$$\int_0^\infty u\ln(u)\tau(u)du < \infty. \tag{B.3}$$

Under this assumption, there exists a random variably W_∞ such that

$$\exp(-rt)Z_t \to W_\infty \text{ almost surely,} \tag{B.4}$$

where r is the Malthusian parameter as defined in Eq. (7) in the main text, and Z_t is the number of infected individuals at time t.

Let A be the non-extinction event. We know that $\mathbf{E}[W_\infty] = 1$ and that almost surely $A = \{W_\infty > 0\}$. It follows that

$$\mathbf{E}[W_\infty|A] = \frac{1}{1-p_{\text{ext}}}, \tag{B.5}$$

where p_{ext} is the extinction probability, which is the smallest root of the probability generating function as defined in Eq. (1) in the main text:

$$p_{\text{ext}} = \mathbf{E}[p_{\text{ext}}^Y]. \tag{B.6}$$

Combining Eqs. (B.4) and (B.5) gives the formal justification for the correction of the initial epidemic size by $1/(1-p_{\text{ext}})$ in Eq. (10) in the main text.

Further, if $\psi(t) = \mathbf{E}[e^{tY}]$ is the Laplace transform (or moment-generating function) of W_∞, then ψ satisfies the fixed point problem (Cohn, 1985, Theorem 4.1)

$$\text{for all } u\geq 0,\ \ \psi(u) = \mathbf{E}\Big[\prod_{i=1}^{Y}\psi(ue^{-rt_i})\Big]. \tag{B.7}$$

Let us now evaluate the variance of W_∞ conditional on non-extinction. Differentiating the Laplace transform ψ twice with respect to u, we get

$$\begin{aligned}\psi''(u) &= \mathbf{E}\Big[\mathbb{1}_{Y\geq 1}\sum_i e^{-2rt_i}\psi''(ue^{-rt_i})\prod_{j\neq i}\psi(ue^{-rt_i})\Big] + \\ &\quad \mathbf{E}\Big[\mathbb{1}_{Y\geq 2}\sum_{i\neq j} e^{-rt_i}e^{-rt_j}\psi'(ue^{-rt_i})\psi'(ue^{-rt_j})\prod_{k\neq i,j}\psi(ue^{-rt_k})\Big]\end{aligned}$$

Evaluating at $u=0$, we get

$$\mathbf{E}[W_\infty^2] = \mathbf{E}[W_\infty^2]\mathbf{E}\Big[\mathbb{1}_{Y\geq 1}\sum_i e^{-2rt_i}\Big] + \psi'(0)^2\mathbf{E}\Big[\mathbb{1}_{Y\geq 2}\sum_{i\neq j} e^{-rt_i}e^{-rt_j}\Big]$$

medRxiv preprint doi: https://doi.org/10.1101/2020.11.17.20233403; this version posted June 7, 2021. The copyright holder for this preprint (which was not certified by peer review) is the author/funder, who has granted medRxiv a license to display the preprint in perpetuity. It is made available under a CC-BY 4.0 International license .

Since $\psi'(0) = 1/(1-p_{\text{ext}})$, this yields

$$\mathbf{E}[W_\infty^2] = \frac{1}{(1-p_{\text{ext}})^2} \frac{\mathbf{E}\left[\mathbb{1}_{Y\geq 2} \sum_{i\neq j} e^{-rt_i} e^{-rt_j}\right]}{1-\mathbf{E}\left[\mathbb{1}_{Y\geq 1} \sum_i e^{-2rt_i}\right]}.$$

With $A = \{W_\infty > 0\}$ as above, which coincides with the event of non-extinction, we find

$$\begin{aligned}\mathbf{E}[W_\infty^2|A] &= \left(\frac{1}{1-p_{\text{ext}}}\right) \frac{\mathbf{E}\left[\mathbb{1}_{Y\geq 2} \sum_{i\neq j} e^{-rt_i} e^{-rt_j}\right]}{1-\mathbf{E}\left[\mathbb{1}_{Y\geq 1} \sum_i e^{-2rt_i}\right]} \\ &= \left(\frac{1}{1-p_{\text{ext}}}\right) \frac{\int_0^\infty \exp(-r(t+u))c(t,u)\,dt\,du}{1-\int_0^\infty \exp(-2rt)\tau(t)\,dt}.\end{aligned}$$

Then

$$\mathbf{Var}[W_\infty^2|A] = \frac{1}{1-p_{\text{ext}}}\left(\frac{\int_0^\infty \exp(-r(t+u))c(t,u)\,dt\,du}{1-\int_0^\infty \exp(-2rt)\tau(t)\,dt} - \frac{1}{1-p_{\text{ext}}}\right).$$

medRxiv preprint doi: https://doi.org/10.1101/2020.11.17.20233403; this version posted June 7, 2021. The copyright holder for this preprint (which was not certified by peer review) is the author/funder, who has granted medRxiv a license to display the preprint in perpetuity. It is made available under a CC-BY 4.0 International license .

C Renewal equation in the absence of conditioning

We informally derive the renewal equation of the incidence and the epidemic size as given in Eqs. (5) and (6) in the main text.

In the following, σ_x denotes the time of infection of individual x and $\mathscr{F}_t$ denotes the history of the infection process up to time t. (In the probabilistic jargon, $(\mathscr{F}_t)_{t\geq 0}$ is the natural filtration associated with the infection process). Let us define the random empirical measure, which counts the number of infections in a small time interval $[t, t+dt]$

$$db(t) = \sum_{x:\sigma_x<\infty} \delta_{\sigma_x}(dt), \tag{C.1}$$

where δ_{σ_x} is the Dirac measure. The random empirical measure db records the infection times along the course of the epidemic. Each atom of the random measure db corresponds to a time of infection. Note that since the epidemic is triggered by a single individual of age 0 at time 0, db has a Dirac mass at 0. For $t>0$, we can assume without loss of generality that $\mathbf{E}[db]$ has no atom and we write

$$\text{for all } t>0, \;\; i(t) := \frac{\mathbf{E}[db(t)]}{dt}, \tag{C.2}$$

where $i(t)$ is the overall rate at which new individuals are infected in a small time interval $[t, t+dt]$. In other words, $i(t)dt$ models the incidence in the time interval $[t, t+dt]$.

Our goal is to show that i satisfies the renewal equation

$$i(t) = \tau(t) + \int_0^t \tau(t-u)i(u)du. \tag{C.3}$$

Informally, we have

$$\mathbf{E}\Big[db(t) \mid \mathscr{F}_t\Big] = \sum_{\sigma_x<t} dt \times \tau(t-\sigma_x). \tag{C.4}$$

In words, if we condition on the history of the process up to time t, the expected number of new infections in the time interval $[t, t+dt]$ can be computed by adding up the expected contribution of every infected individual before time t. For individual x, this expected contribution is $dt\times\tau(t-\sigma_x)$ and the previous equation follows by adding up the contribution of every previously infected individual.

Next, the sum on the right hand side of the latter equation can we rewritten in terms of an integral with respect to the infection measure db in the following way

$$\sum_{\sigma_x<t} dt \times \tau(t-\sigma_x) = dt \int_{[0,t)} \tau(t-u)db(u), \tag{C.5}$$

so that

$$\mathbf{E}\Big[db(t) \mid \mathscr{F}_t\Big] = dt \int_{[0,t)} \tau(t-u)db(u). \tag{C.6}$$

Averaging over every realization of the process up to time t, we obtain

$$\begin{aligned} \mathbf{E}\Big[db(t)\Big] &= dt\, \mathbf{E}\Big[\int_{[0,t)} \tau(t-u)db(u)\Big] \\ &= dt \int_{[0,t)} \tau(t-u)\mathbf{E}[db(u)]. \end{aligned} \tag{C.7}$$

Recalling our definition of $i(t)$ in Eq. (C.2), this yields

$$i(t) = \tau(t) + \int_0^t \tau(t-u)i(u)du, \tag{C.8}$$

medRxiv preprint doi: https://doi.org/10.1101/2020.11.17.20233403; this version posted June 7, 2021. The copyright holder for this preprint (which was not certified by peer review) is the author/funder, who has granted medRxiv a license to display the preprint in perpetuity. It is made available under a CC-BY 4.0 International license .

where the term $\tau(t)$ on the right hand side follows from the fact that db has a Dirac mass at 0. This is Eq. (5) in the main text.

The cumulative epidemic size $I(t) := 1 + \int_0^t i(s)ds$ then satisfies the renewal equation

$$\begin{aligned} I(t) &= 1 + \int_0^t i(s)ds \\ &= 1 + \int_0^t \left(\tau(s) + \int_0^s i(s-u)\tau(u)du\right)ds \\ &= 1 + \int_0^t \tau(s)ds + \int_0^t \tau(u) \int_a^t i(s-u)\tau(u)ds\, du \\ &= 1 + \int_0^t \tau(s)ds + \int_0^t \tau(u) \underbrace{\int_0^{t-u} i(s)ds}_{=I(t-u)-1} du \\ &= 1 + \int_0^t \tau(a)I(t-u)du, \end{aligned} \tag{C.9}$$

where we have used Fubini's theorem to change the order of integration. This explains Eq. (6) in the main text.

medRxiv preprint doi: https://doi.org/10.1101/2020.11.17.20233403; this version posted June 7, 2021. The copyright holder for this preprint (which was not certified by peer review) is the author/funder, who has granted medRxiv a license to display the preprint in perpetuity. It is made available under a CC-BY 4.0 International license .

D Delay differential equation for the process conditioned on explosion

In this section, we derive a delay differential equation for the rate of new infections over time when the process is conditioned on non-extinction. This delay differential equation explains Eq. (12) in the main text.

Markov model. For simplicity, we assume that the infection process is Markovian in its age structure. More precisely, this means that the ages of infection for a given individual are given by a Poisson point process with intensity τ. At time $t > 0$, we encode the population by a random vector $\mathbf{a} = (a_1, a_2, \cdots, a_n)$ where $a_1 > \cdots > a_n$ are the ages of infection listed in decreasing order (individual 1 is the first infected individual etc.), and n is the number of infected individuals at time t. We denote by $|\mathbf{a}|$ the number of elements in $\mathbf{a}$. The infinitesimal generator of the infection process is then given by

$$Lf(\mathbf{a}) \;=\; \sum_{i=1}^{|\mathbf{a}|} \Big[\tau(a_i)\Big(f((\mathbf{a},0)) - f(\mathbf{a})\Big) \;+\; \partial_i f(\mathbf{a})\Big]\,, \tag{D.1}$$

where $(\mathbf{a},0) := (a_1, \cdots, a_{|\mathbf{a}|}, 0)$ and f is a continuous and bounded test function (e.g Ethier and Kurtz, 1986). Intuitively, one can think of the infinitesimal generator to be the expected rate of change of a Markov process, which generalizes the concept of the transition rate matrix in the case of a discrete state continuous time Markov chain. It encodes the infinitesimal dynamics of the branching process in the following way: on a time interval dt,

- an individual of age a_i produces a new infection with a probability $\tau(a_i)dt$. Conditional on this event, the age structure of the population makes a transition from $\mathbf{a}$ to $(\mathbf{a},0)$, i.e., an individual of age 0 is added to the population.
- the age of every individual increases by dt (this corresponds the partial derivative of f in the generator).

The Doob h-transform. Let us now consider the probability of survival, which is equivalent to explosion ($Z_t \to \infty$ for $t \to \infty$),

$$h(\mathbf{a}) \;:=\; 1 - \prod_{i=1}^{|\mathbf{a}|} p_{\text{ext}}(a_i). \tag{D.2}$$

for a population with initial age structure $\mathbf{a}$. Making use of Eq. (A.3), we note that h is a harmonic function for the generator L, i.e., $Lh = 0$. Let us consider the Markov process with infinitesimal generator

$$\widetilde{L}f = \frac{1}{h}L(fh)\,. \tag{D.3}$$

This is the Doob h-transform of the original process.

Branching process conditioned on explosion. The Markov process with generator $\widetilde{L}$ is known to be identical in law with the original process conditioned on explosion (Doob, 1957; Chetrite and Touchette, 2015). Using $Lh = 0$, the transformed infinitesimal generator computes to

$$\begin{aligned}\widetilde{L}f(\mathbf{a}) &= \sum_{i=1}^{|\mathbf{a}|}\left[\tau(a_i)\frac{h((\mathbf{a},0))}{h(\mathbf{a})}\Big(f((\mathbf{a},0)) - f(\mathbf{a})\Big) \;+\; \partial_i f(\mathbf{a})\right] \\ &= \sum_{i=1}^{|\mathbf{a}|}\left[\tau(a_i)\frac{1 - p_{\text{ext}}(0)\prod_{i=1}^{|\mathbf{a}|} p_{\text{ext}}(a_i)}{1 - \prod_{i=1}^{|\mathbf{a}|} p_{\text{ext}}(a_i)}\Big(f((\mathbf{a},0)) - f(\mathbf{a})\Big) \;+\; \partial_i f(\mathbf{a})\right]\end{aligned} \tag{D.4}$$

medRxiv preprint doi: https://doi.org/10.1101/2020.11.17.20233403; this version posted June 7, 2021. The copyright holder for this preprint (which was not certified by peer review) is the author/funder, who has granted medRxiv a license to display the preprint in perpetuity. It is made available under a CC-BY 4.0 International license .

The formula can now be interpreted as follows. For a given age structure **a**, conditioning on explosion induces an adjustment of the infection rate of the ith individual as follows

$$\widetilde{\tau}^{\mathbf{a}}(a_i) \;=\; \tau(a_i) \cdot \underbrace{\frac{1 - p_{\text{ext}}(0)\prod_{j=1}^{|\mathbf{a}|} p_{\text{ext}}(a_j)}{1 - \prod_{j=1}^{|\mathbf{a}|} p_{\text{ext}}(a_j)}}_{\text{adjustment}}. \tag{D.5}$$

We note that the infection rate is increased for every individual, independent of their age of infection, by the same amount. The increase, however, depends on the infection age structure of the entire infected population.

The delay equation. We keep the same notation as in Appendix C. By the same reasoning as in Appendix C, we have

$$\mathbf{E}[db(t)|\mathscr{F}_t] \;=\; \sum_{\sigma_x<t}\Big(\frac{1 - p_{\text{ext}}(0)\prod_{y:\sigma_y<t} p_{\text{ext}}(t-\sigma_y)}{1 - \prod_{y:\sigma_y<t} p_{\text{ext}}(t-\sigma_y)}\Big)\, dt \times \tau(t-\sigma_x)\,. \tag{D.6}$$

In words Eq. (D.6) means that if we condition on the history of the process up to time t, the expected number of new infections in the time interval $[t, t+dt]$ can be computed by adding up the expected contribution of every infected individual before time t. According to Doob's h-transform formula, for an individual infected at time σ_x, the expected contribution of this individual is given by $dt \times \tau(t-\sigma_x)$ multiplied by the Doob's term

$$\Big(\frac{1 - p_{\text{ext}}(0)\prod_{y:\sigma_y<t} p_{\text{ext}}(t-\sigma_y)}{1 - \prod_{y:\sigma_y<t} p_{\text{ext}}(t-\sigma_y)}\Big), \tag{D.7}$$

which depends on the whole age structure of the population up to time t.

We now rewrite the adjustment factor in the following way

$$\begin{aligned}\frac{1 - p_{\text{ext}}(0)\prod_{y:\sigma_y<t} p_{\text{ext}}(t-\sigma_y)}{1 - \prod_{y:\sigma_y<t} p_{\text{ext}}(t-\sigma_y)} &= \frac{1 - p_{\text{ext}}(0)\exp\Big(\sum_{y:\sigma_y<t}\ln(p_{\text{ext}}(t-\sigma_y))\Big)}{\exp\Big(\sum_{y:\sigma_y<t}\ln(p_{\text{ext}}(t-\sigma_y))\Big)}\\ &= \frac{1 - p_{\text{ext}}(0)\exp\Big(\int_{[0,t)}\ln(p_{\text{ext}}(t-u))db(u)\Big)}{1 - \exp\Big(\int_{[0,t)}\ln(p_{\text{ext}}(t-u))db(u)\Big)}.\end{aligned} \tag{D.8}$$

As a consequence, Eq. (D.6) can be rewritten as

$$\begin{aligned}\mathbf{E}[db(t)|\mathscr{F}_t] &= dt\Big(\sum_{x:\sigma_x<t}\tau(t-\sigma_x)\Big) \times \frac{1 - p_{\text{ext}}(0)\exp\Big(\int_{[0,t)}\ln(p_{\text{ext}}(t-u))db(u)\Big)}{1 - \exp\Big(\int_{[0,t)}\ln(p_{\text{ext}}(t-u))db(u)\Big)}\\ &= dt\int_{[0,t)}\tau(t-u)db(u) \times \frac{1 - p_{\text{ext}}(0)\exp\Big(\int_{[0,t)}\ln(p_{\text{ext}}(t-u))db(u)\Big)}{1 - \exp\Big(\int_{[0,t)}\ln(p_{\text{ext}}(t-u))db(u)\Big)}.\end{aligned} \tag{D.9}$$

Averaging over the past of the infection process $\mathscr{F}_t$, we find that

$$\mathbf{E}[db(t)] = \quad dt\,\mathbf{E}\Big[\int_{[0,t)}\tau(t-a)db(a) \times \frac{1 - p_{\text{ext}}(0)\exp\Big(\int_{[0,t)}\ln(p_{\text{ext}}(t-a))db(a)\Big)}{1 - \exp\Big(\int_{[0,t)}\ln(p_{\text{ext}}(t-a))db(a)\Big)}\Big]. \tag{D.10}$$

medRxiv preprint doi: https://doi.org/10.1101/2020.11.17.20233403; this version posted June 7, 2021. The copyright holder for this preprint (which was not certified by peer review) is the author/funder, who has granted medRxiv a license to display the preprint in perpetuity. It is made available under a CC-BY 4.0 International license .

Since db has a Dirac at 0 we have

$$\mathbf{E}[db(t)] = \quad dt\mathbf{E}\Big[\Big(\tau(t) + \int_0^t \tau(t-u)db(u)\Big) \times \frac{1 - p_{\text{ext}}(0)p_{\text{ext}}(t)\exp\Big(\int_0^t \ln(p_{\text{ext}}(t-u))db(u)\Big)}{1 - p_{\text{ext}}(t)\exp\Big(\int_0^t \ln(p_{\text{ext}}(t-u))db(u)\Big)}\Big]. \tag{D.11}$$

Let us now compare this formula with its analog in Eq. (C.7) in the absence of conditioning the process on survival. In Eq. (C.7), we can use Fubini's theorem to interchange the integral and the expected value. This provides the renewal equation for the average infection measure $i(t)$ – see Eq. (C.3). In the presence of conditioning in Eq. (D.11), the right hand side is not linear in db anymore and we cannot derive an autonomous equation for the density $i(t)$ as in the unconditioned case. Our approximation now consists in ignoring the non-linearities on the right hand side of Eq. (D.11) and replacing $db(t)$ by its expected value. This gives

$$\begin{aligned}\widetilde{i}(t) &= \Big(\tau(t) + \int_0^t \tau(t-u)\widetilde{i}(u)du\Big) \times \frac{1 - p_{\text{ext}}(0)p_{\text{ext}}(t)\exp\Big(\int_0^t \ln(p_{\text{ext}}(t-u))\widetilde{i}(u)du\Big)}{1 - p_{\text{ext}}(t)\exp\Big(\int_0^t \ln(p_{\text{ext}}(t-u))\widetilde{i}(u)du\Big)} \\ &= F(\widetilde{i}(s); s \in [0,t]),\end{aligned} \tag{D.12}$$

which explains Eq. (12) in the main text. The overall epidemic size of the conditioned process is then given by $\widetilde{I}(t) = 1 + \int_0^t \widetilde{i}(s)ds$.

medRxiv preprint doi: https://doi.org/10.1101/2020.11.17.20233403; this version posted June 7, 2021. The copyright holder for this preprint (which was not certified by peer review) is the author/funder, who has granted medRxiv a license to display the preprint in perpetuity. It is made available under a CC-BY 4.0 International license .

E Cumulative epidemic size over time

In the main text, we have seen that the cumulative epidemic size over time varies a lot between different stochastic simulations (Fig. 2). The number of secondary infections was Poisson-distributed in the main text. The negative binomial distribution exhibits more variance than a Poisson distribution. Therefore, the variance of the cumulative epidemic size obtained from 10,000 stochastic simulations is even larger in this case (compare the subfigures in Fig. A). This can be explained as follows: First, super-spreading events are more likely and as a result, epidemic sizes can be much larger. Secondly, and conversely, a larger number of infected individuals do not transmit the infection at all; as a result, the total epidemic size can remain smaller.

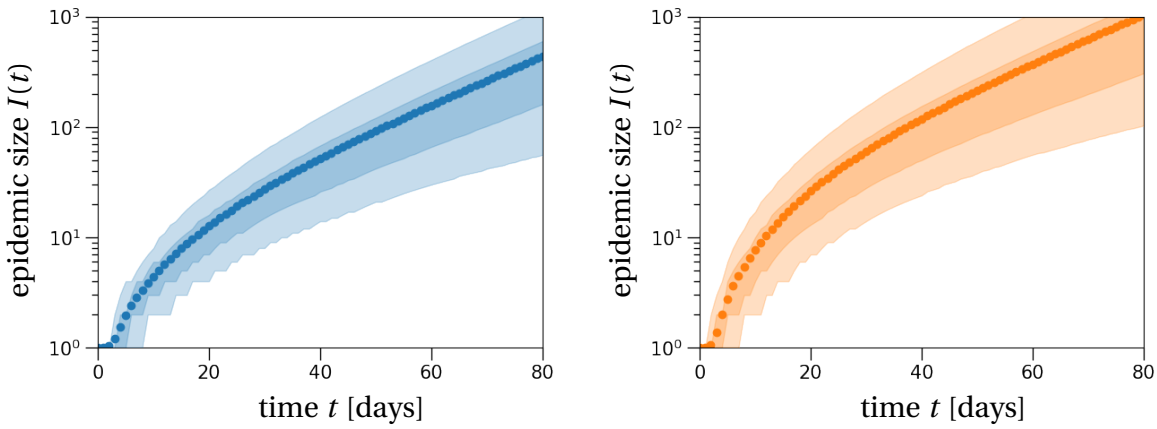

(a) Poisson

(b) negative binomial

Figure A: **The cumulative number of infected individuals over time.** The light and dark shaded regions show the 90% and 50% inter-quantile ranges obtained from 10,000 stochastic simulations that resulted in establishment of an epidemic cluster. Dots represent the average of these simulations over time. With a negative binomial offspring distribution (b), a lot of infected individuals do not transmit the disease, which results in lower epidemic sizes than compared to a Poisson offspring distribution (a). In contrast, few infected individuals with a lot of secondary infections early in the epidemic can generate much larger epidemic sizes when compared to the Poisson distribution. These two effects together explain the much larger variance in epidemic sizes for the negative binomial distribution compared to the Poisson distribution. The effective reproduction number is set to $R = 1.3$ and the transmission density $\mu(t)$ is a Gamma distribution with the parameters as stated in Table 1 in the main text.